Engineering Structures 172 (2018) 382–391

Contents lists available at ScienceDirect

Engineering Structures

journal homepage: www.elsevier.com/locate/engstruct

A comparative study on nonlinear models for performance-based earthquake engineering

Rafael A. Salgado*, Serhan Guner

Department of Civil Engineering, University of Toledo, Toledo, OH 43607, USA

ARTICLE INFO

Keywords:
Nonlinear analysis
Reinforced concrete
Frame structures
Performance-based earthquake engineering
Dynamic analysis
Shear-critical structures
Computational demand

ABSTRACT

Performance-based earthquake engineering requires a large number of nonlinear dynamic analyses to statistically assess the performance of frame structures. The complexity and high computational demand of such procedures, however, has hindered its use in practice. The objective of this study is to evaluate the performance of three numerical models with varying computational demand levels. Two nonlinear models with different complexities and one linear model with a concentrated plasticity approach were used to evaluate a reinforced concrete frame. The accuracy of the calculated responses was assessed using the experimental results. A total number of 126 dynamic analyses were performed to derive fragility curves. The nonlinear models calculated significantly more accurate structural responses than the more-commonly used plastic-hinge model. The model preparation and result acquisition times were found to comprise a significant portion of the total computational demand of each model. An overview of the performance-based modeling processes and the critical points for minimizing the computational demand while retaining the calculation accuracy are also presented.

1. Introduction

Performance-based earthquake engineering (PBEE) makes use of the nonlinear structural analysis (NLA) methods to accurately predict the inelastic response that most buildings undergo during seismic excitation. Amongst different NLA methods, the nonlinear dynamic analysis (NLDA) methods, also known as time-history analysis, provide the most realistic simulation of structural behavior [1–4]. Multiple NLDAs are required to assess (or design) a structure using PBEE; however, the NLDA methods are complex and computationally-intensive, which significantly limits their applicability in practical situations.

Previous studies have either focused on proposing simplified analysis procedures [4–9] to substitute the need for the NLDA methods or evaluate the influence of local element assumptions and modeling approaches on the overall structural response [10–12]. There is still a lack of studies that investigate the structural response reliability when a structural system is numerically analyzed with different modeling techniques. The objective of this research is to study various numerical modeling techniques with different complexity levels and evaluate their simulation accuracy and computational demand. For this objective, a PBEE structural assessment of a previously-tested RC frame is conducted using three modeling approaches. The calculated structural risk to a set of performance limits is evaluated by means of fragility curves.

2. Performance-based earthquake engineering

A summary of the PBEE structural assessment is presented herein to illustrate the methodology used in this paper [13,14]. First, the building location, importance, and soil condition are used to determine the earthquake hazard level and the response spectrum of the structure as per the applicable building code. Structural analysis is then conducted using a numerical model subjected to a series of ground motion (GM) acceleration histories that match the response spectrum. The performance is evaluated based on the calculated responses and the structural risk is expressed by means of fragility (or vulnerability) curves, which indicate the probability of the structure to exceed a certain damage state (i.e., damage measures or performance levels) based on the engineering demand parameters (EDP) (e.g., story drift, floor accelerations, or velocities) calculated by the structural analysis. A loss analysis is finally conducted, based on the previously calculated probability of exceedance, to quantify the financial, downtime, casualty, or other types of loses.

3. Hazard determination

In this study, the structure considered is in Portland, Oregon, USA, and constructed over ‘type D’ soil, which is the standard soil type in ASCE 7 [15] when no sufficient detail is provided. The design response

* Corresponding author.
E-mail addresses: rafael.salgado@rockets.utoledo.edu (R.A. Salgado), serhan.guner@utoledo.edu (S. Guner).

https://doi.org/10.1016/j.engstruct.2018.06.034
Received 21 April 2017; Received in revised form 5 April 2018; Accepted 7 June 2018

Table 1
Selected ground motion characteristics.

ID	Earthquake name	Year	Station name	Mag.	Epicenter distance, km	Scale factor
1	Imperial Valley-02	1940	El Centro Array #9	6.95	12.98	1.5
2	Imperial Valley-06	1979	Agrarias	6.53	2.62	2.6
3	Victoria, Mexico	1980	Cerro Prieto	6.33	33.73	1.2
4	Superstition Hills-02	1987	El Centro Imp. Co. Cent	6.54	35.83	1.6
5	Landers	1992	Desert Hot Springs	7.28	27.32	2.7
6	Erzican, Turkey	1992	Erzincan	6.69	8.97	1.5
7	Parkfield-02, CA	2004	Parkfield - UPSAR 13	6.00	12.59	2.6

spectrum was calculated based on the NEHRP [16] provisions.

Seven acceleration histories were considered to meet the minimum requirements of the NEHRP [16] provisions. The ground motion characteristics included: 'strike-slip' fault type, less than 50 km to the epicenter, and Richter magnitude between 6 and 8 (see Table 1). Time-histories were obtained from the Pacific Earthquake Engineering Research (PEER) online NGA-West2 database [17].

The selected ground motions were scaled such that the average follows the requirements of NEHRP [16], with the result shown in Fig. 1. The one-third scale frame to be examined exhibited a natural period of 0.303 s, which corresponds to a full-scale period of 0.525 s.

4. Structural analysis

A structure designed based on pre-1970 s building codes was chosen for assessment using the PBEE methods due to their seismically-deficient details. The frame examined was a one-third scale, three-story, three-bay planar structure designed by Ghannoum and Moehle [18] to develop a flexure-shear-critical failure mechanism (i.e., the columns yield in flexure prior to a shear failure). Two of the columns were constructed with widely-spaced shear reinforcement (denoted as non-ductile columns), while the other two columns were designed to fulfill ACI 318-08 specifications (denoted as ductile columns). Ghannoum and Moehle [18] indicated that the mixture of older-type columns and ductile columns is not completely representative of typical 1970s construction. It was introduced in the test frame so that collapse of the frame due to the failure of the older-type columns would be slowed by the ductile columns and the dynamic failure mechanism could be more closely monitored. A strong beam-weak column mechanism was included, and the beam-column joints were designed in accordance with ACI 318-08 to avoid any joint failure prior to a column failure. Each beam carried 26.68-kN lead weight packets distributed over two points located approx. 0.4 m from the face of each column. A sketch of the frame is shown in Fig. 2.

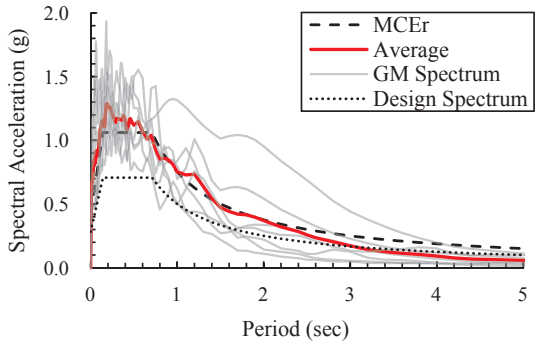

Fig. 1. Spectral response.

The frame was subjected to four shake table tests using the March 3, 1985, Chile Earthquake (Llolleo Station, Component 100); namely, half-yield (HY), and dynamic tests 1, 2, and 3 (DT1, DT2, and DT3). Table 2 lists the ground motion scale factors and the response of the frame in each test [18].

5. Numerical modeling

In this study, three numerical models were created. A full nonlinear model that employs distributed-plasticity fiber-based elements, called Nonlinear Fiber-Based (NLFB) model; a simplified nonlinear model with fewer and longer flexure-only elements with combined shear-hinges, called Nonlinear Fiber-Based Shear Hinge (NLFBSH) model; and a fully-elastic model with concentrated flexure, axial, and shear-hinges, called Elastic with Concentrated Plasticity Hinges (ECPH) model. All models used two-dimensional beam-column elements due to their computational efficiency and analytical accuracy.

5.1. Nonlinear fiber-based model (NLFB)

The NLFB model employed the frame element developed by Guner and Vecchio [19]. This element performs interrelated global and sectional analyses, where the internal forces calculated by the former are used to perform the latter. It is based on the Modified Compression Field Theory (MCFT) [20], which allows the element to account for the coupled flexure, axial and shear effects. Additionally, the MCFT uses the average and local strains and stresses of the concrete and reinforcement, and the widths and orientations of cracks throughout the load-deformation response of the element. Shear strains are calculated using a parabolic strain distribution [19]. The element employs a smeared, rotating crack approach based on a total load, secant stiffness formulation. The triaxial concrete core confinement is inherently accounted for through the use of in- and out-of-plane reinforcement ratios. In addition, it incorporates several second-order material behaviors that are specific to reinforced concrete structures, as listed in Table 3 [21].

The structure was modeled using the computer program VecTor 5 [22,23]. The structural analysis package also incorporates graphical pre- and post-processor programs. FormWorks Plus [24,25] is a graphical pre-processor developed specifically for the VecTor suite of applications to provide better modeling capabilities such as the list of available elements and material models, auto-meshing and auto-substructure features. The post-processor program Janus [26,27] can display the displaced shape of the structure, crack widths, locations and propagation, rebar and concrete stresses and strains, and failure conditions. The post-processor program is a critical component of structural assessment process since they aid analysts to understand the structural behavior, detect modeling mistakes, and effectively compare the calculated responses. Some important capabilities of the computer program VecTor5 are summarized in Table 4.

The concrete uniaxial stress-strain response was modeled using the Popovics and Modified Park-Kent models for the pre- and post-peak responses [21]. The steel reinforcement stress-strain response is composed of three parts: linear-elastic response, yield plateau, and a nonlinear strain-hardening phase until rupture in tension, and a buckling response in compression (see Fig. 3). As recommended by [19], each beam and column was divided into elements of about half of its cross-section height (see Fig. 4), and the number of fibers used in all cross-sections was kept at about 30 fibers. The longitudinal reinforcement was discretely modeled while the shear reinforcement was smeared into relevant concrete layers.

The NLFB model incorporated a nonlinear concrete model with plastic offsets proposed by [28]. In this model, the concrete unloads to a plastic offset strain, not to the origin of the stress-strain diagram, following a nonlinear Ramberg-Osgood formulation. The reinforcing steel hysteretic response was based on the Seckin model with Bauschinger

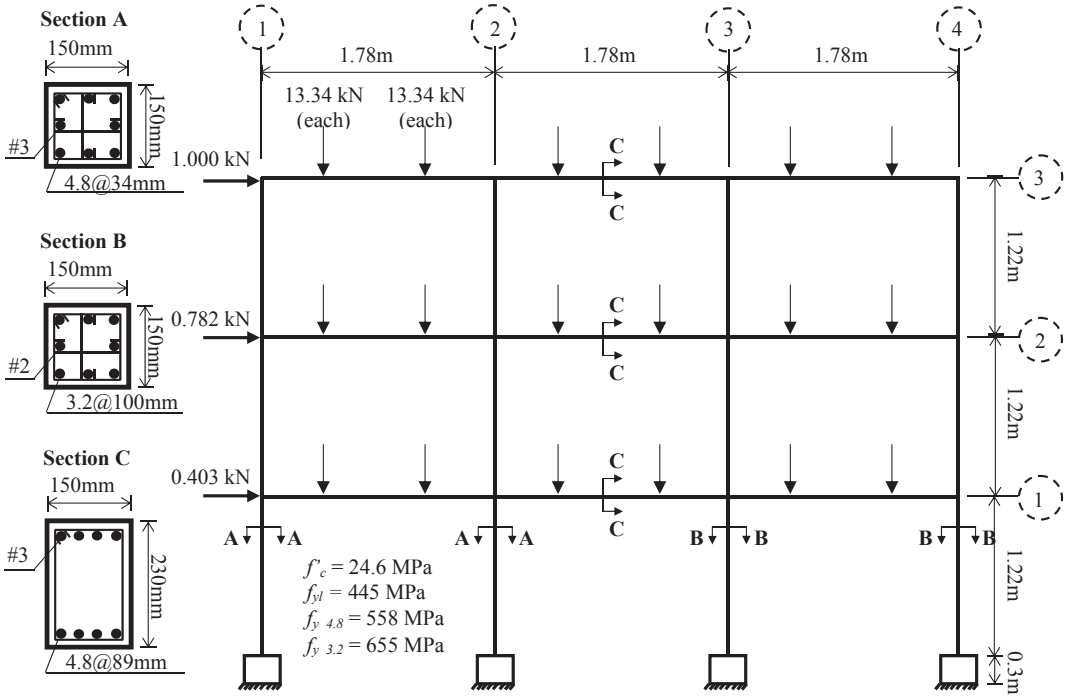

Fig. 2. Frame and section design details.

Table 2
Dynamic tests and respective ground motion scale factor.

Test	GM scale factor	Frame response
HY	0.3625	Minor flexural cracks
DT1	4.06	Column 3 shear and axial failure at 5.2% story drift
DT2	4.06	Column 4 advanced shear damage. No failure
DT3	5.80	Column 4 failure. Partial collapse of frame's east side

Table 3
Material models and second-order behaviors considered.

Material behavior	Default model
Compression softening	Vecchio 1992-A
Tension stiffening	Modified Bentz 2003
Tension softening	Linear
Confinement strength	Kupfer/Richart
Crack width check	Max crack width of Agg/5
Rebar dowel action	Tassios (Crack slip)
Rebar buckling	Refined Dhakal-Maekawa

effect [29] in tension, and the refined Dhakal-Maekawa model for compression [21] as shown in Fig. 3. The primary energy dissipation mechanism considered in this study occurred due to the nonlinear hysteretic material constitutive models incorporated in each numerical model. Consequently, no additional damping was necessary, due to the fully nonlinear elements of the NLFB model. However, for all the models in this study, the dynamic analyses were performed based on the average Newmark integration method, which typically requires a minimal amount of damping for numerical stability. The NLFB model achieved numerical stability with a Rayleigh damping ratio of 0.5% for the first two modes, in addition to an inherent hysteretic damping.

5.2. Nonlinear fiber-based shear-hinge model (NLFBSH)

The NLFBSH model was utilized in this study to serve as a simplification of the NLFB model. Consequently, fewer and longer elements were included with a simplified material model formulation. The material constitutive models incorporated the flexure and axial effects only. Second-order reinforced concrete material behaviors were not included (see Table 4). To account for the shear effects, localized shear-hinges were incorporated (see Fig. 4). These simplifications were made to reduce the computational effort while still modeling the critical global structural response mechanisms.

The mesh consisted of closely-spaced elements in series with uncoupled shear-springs at the ends of the beams and columns (i.e., the regions where most of the inelastic deformation was likely to occur). Longer elements were used in between the ends of the beams and columns due to the reduced inelastic response of these regions (see Fig. 4). This mesh layout was based on a study conducted by Leborgne and Ghannoum [30].

The model was developed in OpenSees [31]. OpenSees is the only structural analysis package in this study with no pre- or post-processor capabilities. The output is given in a numbered-list, text-file format, leaving the interpretation to the discretion of the analyst. Additionally, the program requires input text files written in the *tcl* programming language, which greatly limits the use of OpenSees to researchers and expert engineers with significant knowledge on computer programming

Table 4
Summary of each computer programs capabilities.

	Nonlinear analysis	Coupled interaction	Second-order	Monotonic	Dynamic/cyclic	Pre-processor	Post-processor	Organized manual
VecTor 5	✓	F-A-S	✓	✓	✓	✓	✓	✓
OpenSees	✓	F-A		✓	✓			
SAP2000		F-A		✓	✓	✓	✓	✓

F – Flexure; A – Axial; S – Shear.

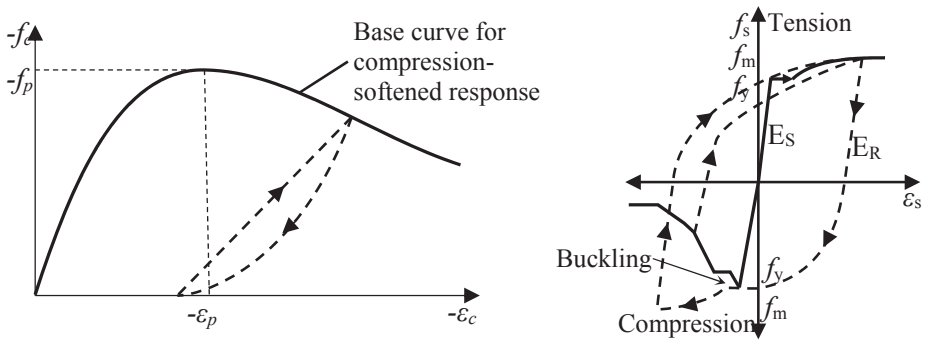

Fig. 3. NLFB hysteretic concrete and steel reinforcing material models.

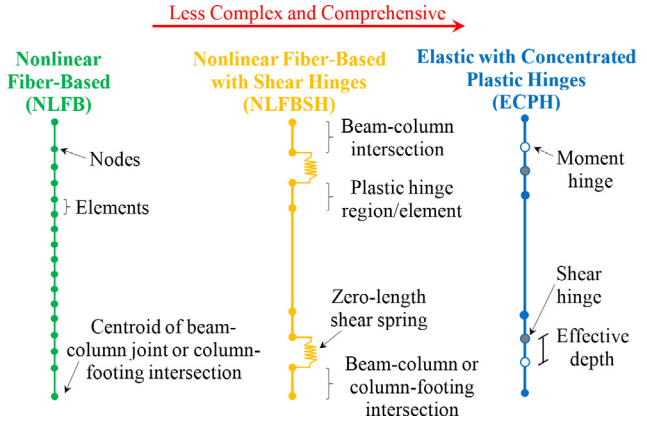

Fig. 4. Beam-column element model approaches.

and nonlinear structural modeling (see Table 4).

The constitutive model of the shear-hinge developed by Leborgne and Ghannoum [30] was employed based on the rotation of the plastic-hinge element (see Fig. 4). The spring exhibits stiffness degradation with hysteretic and pinching cyclic response, as shown in Fig. 5. The rotation-based shear failure was based on an element which yields in flexure prior to a shear failure. The nominal shear strength was calculated as per ASCE 41 [32], with 20% residual strength, and the degradation stiffness was calculated using a regression model calibrated with 56 flexure-shear-critical column experiments. The plastic-hinge length was conservatively chosen to be 1.5 times the cross-section height to contain the plastic rotation [30].

The concrete constitutive compressive stress-strain distribution was modeled using the Hognestad parabola and linear models for the pre- and post-peak responses [33]. OpenSees does not automatically consider concrete confinement due to shear reinforcement. Thus, the core

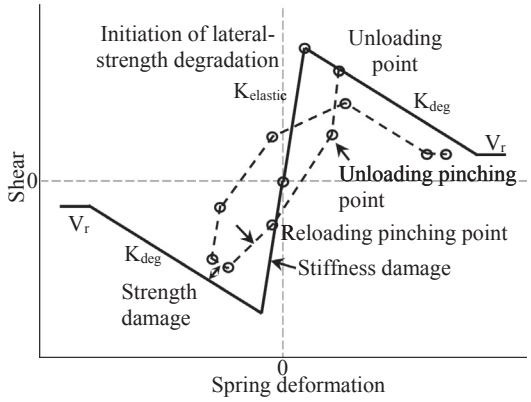

Fig. 5. Shear-hinge nonlinear model [30].

concrete properties had to be calculated using a suitable model [34]. The longitudinal steel reinforcement was discretely modeled with the three-partite stress-strain response, similar to the NLFB model (see Fig. 6a).

The NLFBSH model employed a trilinear concrete hysteresis model with pinching effects developed by Filippou [33]. The concrete unloads to a plastic strain following a linear path. The reinforcing steel hysteretic model was incorporated using the Menegotto-Pinto model (see Fig. 6a). A Rayleigh damping ratio of 3% for the first two modes was required for numerical stability, in addition to the hysteretic damping. The damping ratio used in the NLFBSH model was considerably higher than the ratio used in the NLFB model (i.e., 0.5%) due to the reduced number of elements, the simpler constitutive models, and the mix of nonlinear (i.e., full hysteretic behavior) and linear elements (i.e., no hysteretic behavior) employed by the NLFBSH model.

5.3. Elastic with concentrated plasticity hinges model (ECPH)

The ECPH model was the simplest model considered in this study to evaluate the accuracy of the linear-elastic models with concentrated plasticity hinges under dynamic loads. In this model, each beam or column was modeled using linear-elastic elements. The concentrated-plasticity hinges were the only mechanism that simulated material's nonlinear behavior of the elements. Geometric nonlinearities were included based on large displacement and P-delta effects. The constitutive model of the hinges was derived as per the recommendations in ASCE 41 [32] (see Fig. 6b). In this model, point B represents hinge yielding; point C represents the ultimate capacity of the hinge; and points D and E represents the residual strength and total failure conditions, respectively. ASCE 41 [32] defines three building performance levels: immediate occupancy (IO), life safety (LS), and collapse prevention (CP), as shown in Fig. 6b. Despite the nonlinear behavior of the hinge, the concentrated-plasticity hinges do not typically account for the nonlinear state of the element; rather, they limit the load capacities of the elements (i.e., moment, shear, or axial) at the specific location at which they are placed.

The model was developed using the computer program SAP2000 [35]. The SAP2000 package includes powerful pre- and post-processing capabilities (see Table 4). However, since the focus of the program is on elastic analysis of structures, these tools are limited to structural information predominant of elastic models. SAP2000 post-processor displays the deformed shape of the structure, element forces diagrams, and hinge response with distinct hinge colors. No cracking information is displayed (i.e., the elastic elements do not simulate the cracked conditions) and no concrete or reinforcement stress-strain response is calculated.

The coupled flexural-axial and uncoupled shear-hinges were used in the beam-column elements. The flexure-axial hinge response was used as automatically calculated by SAP2000, which is based on ACI 318-02 [35]. The shear-hinge response, on the other hand, was manually calculated to conform with the newer ACI 318 [36]. Flexure-axial

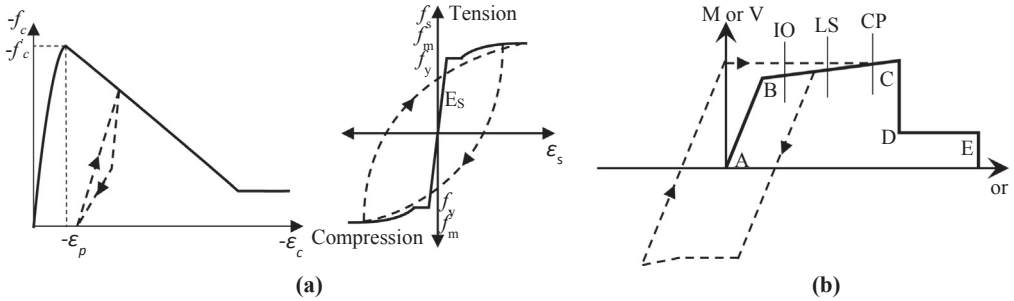

Fig. 6. (a) NLFBSH hysteretic concrete and steel reinforcing material models; (b) ECPH hysteretic model.

interaction hinges were incorporated at the face of the beam-column or column-footing interfaces. Shear-hinges were placed *d* away (i.e., the effective depth of the element) from the beam-column or column-footing interface as per ACI 318 [36] (see Fig. 4). For the hinge lengths, CSI [35] recommends a moment-hinge length to be equal to the cross-sectional height. However, no information is given for the shear-hinge lengths. A shear-hinge length of 1.5 times the cross-section height was adopted as in the NLFBSH model. To account for the cracked conditions of the members, the moment of inertia of the elements was reduced by factors of 0.35 and 0.7 for beams and columns, respectively, as per ACI 318 [36].

The ECPH model employed no hysteretic material behavior in its linear-elastic elements. Only the nonlinear-hinges exhibited a simple hysteretic response. The hysteretic model of the hinges followed a linear path as shown in Fig. 6b. By default, SAP2000 limits the unloading of the hinge (i.e., CDE path in Fig. 6b) to follow a negative stiffness path of 10% the elastic stiffness of the hinge (i.e., AB path in Fig. 6b). This limitation is intended to avoid 'unrealistic' sudden strength loss of strength of ductile elements. However, due to the brittle nature of the shear-hinge, sudden strength loss represents the realistic behavior. Thus, brittle failure of the shear hinges was considered using the recommended element subdivision of 2% or 0.02 [35]. A Rayleigh damping ratio of 5% was used for the first two modes as per ASCE 41 [32] due to the fully-elastic elements employed.

5.4. Mechanisms not included and study limitations

The beam-column joint and bar-slip damage mechanisms should be included in the numerical models of the pre-1970 s structures. However, the joints of the frame examined in this study were designed as per the modern seismic codes to prevent beam-column joint failures. Consequently, rigid end offsets were incorporated in the beam-column and column-footings connections in this study.

The results presented in the following sections were obtained from the analyzed structure only, which is a limitation of this study. To make the obtained results more generally applicable, the authors have limited the number of assumptions to a minimum (as per the previous discussions in this section) while the modelling processes, analysis methodologies, and material models used followed generally considered reinforced concrete structure's methods. The specific numerical results calculated in this study were not taken as definitive but were rather used to establish a comparative relationship between the examined methods.

6. Numerical models calculated response

A dynamic time-history analysis was performed to evaluate the simulation accuracy of the developed models. The dynamic acceleration-history was obtained from the shake table tests performed by Ghannoum and Moehle [18]. To increase the convergence and accuracy of the calculated results, each data point of the experimentally recorded shake-table time-history data was linearly divided into 100 sub-steps [37]. The calculated results were compared with the experimental values in terms of the base shear, first-story drift, damage progression, and failure conditions.

The NLFB and the NLFBSH models were subjected to the half-yield test so that the cracked structural condition could be included at the start of the dynamic test 1. The half-yield test does not affect the ECPH model since it does not simulate cracking in its members. The first-story drift and base shear responses of each model in dynamic test 1 are shown in Fig. 7. The drift was calculated as the average of the displacements of the nodes at the first-floor level divided by the height of the first-floor.

The NLFB and the NLFBSH models failed at the first story level of

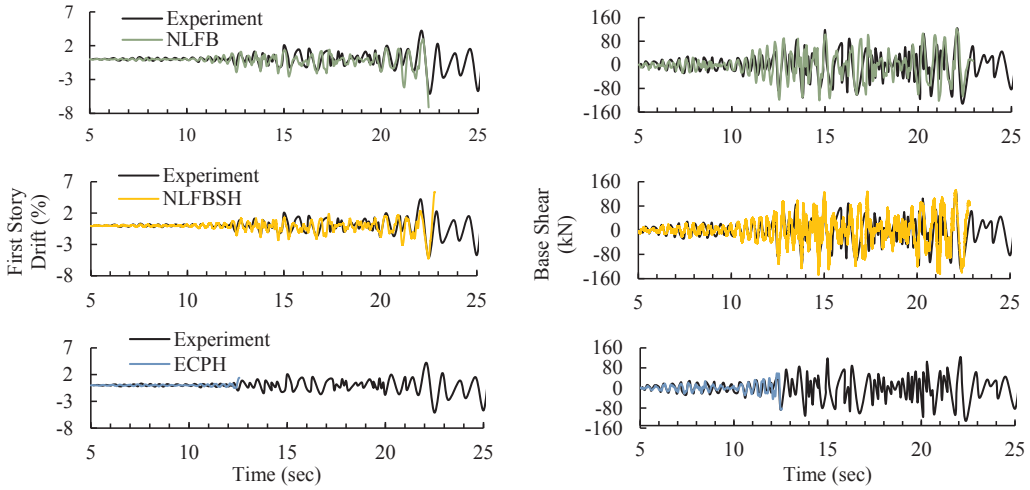

Fig. 7. Numerical models and experimental first-story drift and base shear responses for dynamic test 1.

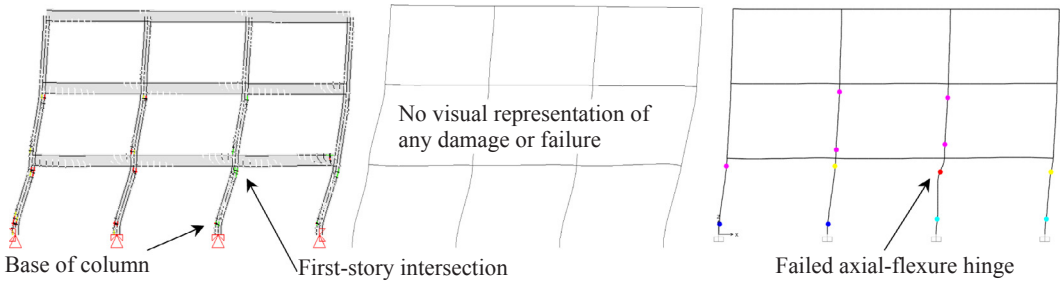

Fig. 8. Failure load stage for a) NLFB, b) NLFBSH, and c) ECPH models.

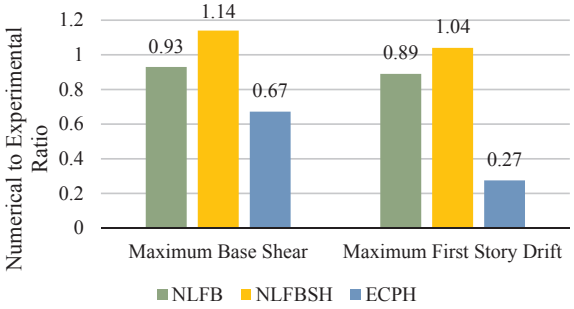

Fig. 9. Numerical to experimental ratio in dynamic test 1.

column 3 at a time of approx. 22 s (see Figs. 7 and 8), which correlated well with the 22.5 s at which the shear failure occurred in the experiment. Furthermore, the calculated first-story drift and base shear values corresponded reasonably well to the experimental response with the calculated-to-experimental discrepancies below 15%, as shown in Fig. 9. The ECPH model failed at a significantly lower time of 12.6 s (see Fig. 7) and calculated the highest deviation from the experimental response (see Fig. 9). The maximum calculated drift ratio corresponded to 27% of the maximum experimental response and the base shear resistance was 67% of the resistance obtained experimentally. The ECPH model resulted in a significant underestimation of the structural capacity due to the failure of the moment hinge at the first story level of column 3 (see Fig. 8). Note that the failure calculated by the ECPH model could not capture the lack of shear capacity of the specimen. The use of code-prescribed axial-flexure and shear resistances, used for the plastic hinges capacities, could not accurately predict the response of the building during the dynamic load.

Fig. 10 shows the hysteresis responses obtained from each model and the envelope of the experimental response. The NLFB and the NLFBSH models satisfactorily captured the experimental responses. The ECPH model calculated a slightly stiffer response due to the use of the cracked moments of inertia for the columns and beams, as per ACI 318 [36]. The hysteretic response of the ECPH model stopped at the failure of the moment hinge shown in Fig. 8. The inability of the numerical model to account for the force redistribution after the hinge failure resulted in a numerical instability and terminated the entire analysis (see Fig. 10).

6.1. Time demand

The total time demanded by a numerical analysis can be divided into three phases: the development time, the analysis time, and the results acquisition time. The development time is the time required to develop and create the model, i.e., selecting the appropriate material models, element types, creating nodes, element connections, applying loads, etc. The analysis time is the time required for the computer to execute the structural analysis. The results acquisition time is the time required to understand the analysis results, such as the failure modes, failure progression, stresses, strains, etc., and extract several types of data to create load versus deflection and other plots. While the analysis time is a pure computational process, with no analyst involvement, the model development and result acquisition times demand significant hands-on effort from the analyst. Consequently, the consideration of the model development and result acquisition times is critical when assessing the practicality of any numerical analysis procedure.

In Fig. 11, the total time demanded by each numerical model developed in this study is presented. The time required by each model was visually broken down into the three phases discussed above. It should be noted that the model development and result acquisition times will vary from analyst to analyst. In this study, these times were consistently obtained by a single analyst with similar levels of previous experience with each software program used.

The numerical model with the highest computational time demand was the NLFBSH model due to the very high model development time (i.e., approx. 80 h). This was caused by the lack of any user interface such as a pre-processor program, and limited and inconsistent users' manual for the use of available elements and models. These drawbacks made the modeling process difficult and tedious, requiring the analyst to make use of trial-and-adjustment methods in the model preparation phase, which significantly increased the time demanded. In general, a user-friendly interface and a well-presented and comprehensive documentation are essential in minimizing the model development time and modeling mistakes. Both the NLFB and ECPH models possessed these features, which translated into a much lower model development time of approx. 8 and 4 h, respectively.

The analysis time required by the numerical models was, as expected, directly proportional to the comprehensiveness level of each model. The type of the analysis performed was also highly influential on the analysis time demand. The time-history dynamic analyses, for example, required significantly more analysis time due to the large number of acceleration points considered. The half yield and the dynamic test 1 were comprised of 900 and 1500 thousand acceleration points, respectively. For each of these points, iterations were performed to achieve numerical convergence by means of matrix algebra; the analysis time spent on each iteration was directly proportional to the stiffness matrix size and the material modeling formulation. Consequently, the NLFB model, which considered the most comprehensive material modeling and employed the highest number of nodes and elements (see Fig. 4), required the highest analysis time of approx. 22 h (see Fig. 11). The NLFBSH model and the ECPH model had the second and third longest analysis time of approx. 2.7 and 0.08 h (i.e., 5 min), respectively. All analyses were performed on an Intel® Core™ i5-2500 quad-core 3.3 GHz CPU with 8 GB DDR3 1333 MHz RAM.

The result acquisition time, similarly to the model development time, highly depended on the availability of a graphical post-processing program. Consequently, the model with the highest result-acquisition time was the NLFBSH model with approx. 5 h. In addition to the drawbacks mentioned for the model development time, the NLFBSH model output the analysis results in text files, which required additional effort from the analyst to translate and interpret the tabulated results into meaningful structural response information. The availability of powerful post-processing tools for both the NLFB and ECPH models

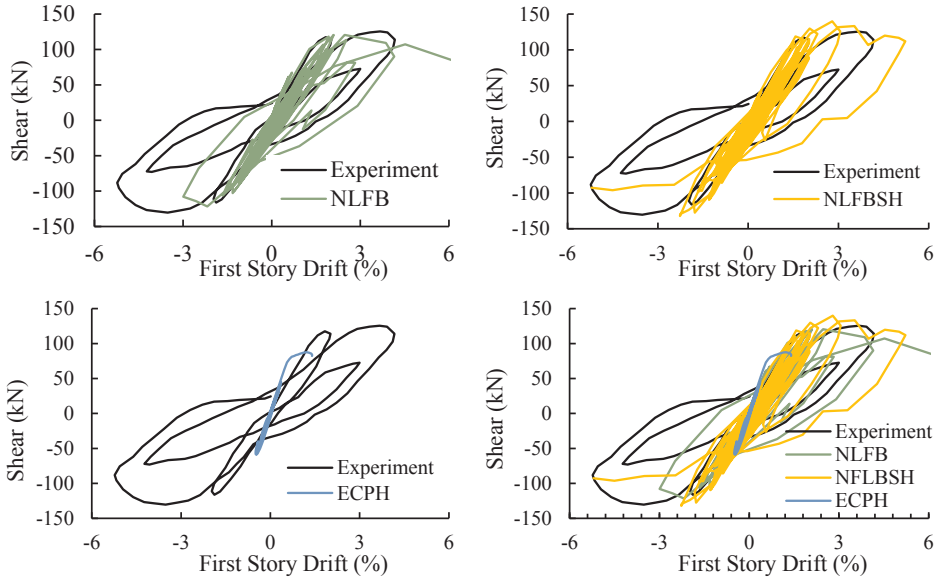

Fig. 10. Numerical models and experimental hysteresis response.

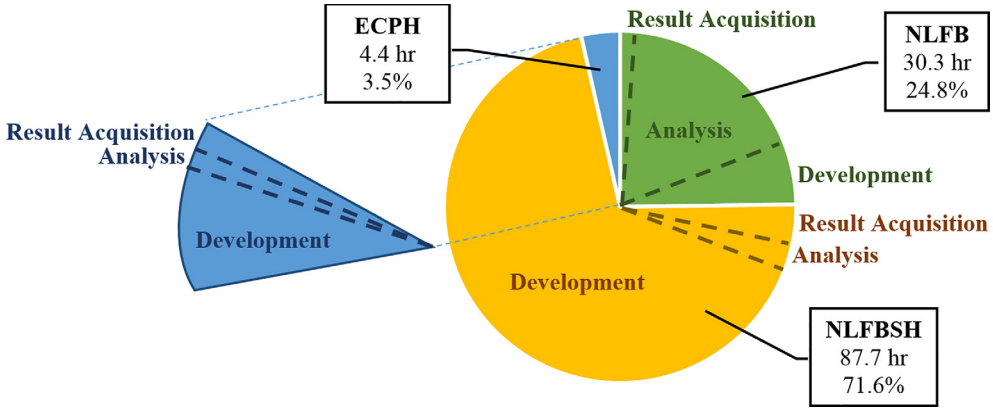

Fig. 11. Total time demanded by each numerical model.

resulted in a significantly lower result acquisition time of approx. 0.5 and 0.3 h, respectively (see Fig. 11), and encouraged a more thorough examination of the analysis results.

7. Performance assessment and fragility functions

Fragility functions, which defines the probability of incurring a performance limit as a function of ground motion intensity [14], were derived to study the probability of exceeding the performance levels considered in this study. The performance of the structure was quantified by comparing the calculated engineering demand parameters (EDP), in terms of maximum first-story drift (θ_{max}), to the three performance levels of immediate occupancy (IO), life safety (LS), and collapse prevention (CP) as per ASCE 41 [32]. The spectral acceleration, S_a, was chosen as the intensity measure parameter for the ground motions.

The choice of which damage measure the structure is going to be assessed for is a subject that depends on regulatory agencies, code specifications, and the building owner requirements. The maximum drift ratio for the IO is commonly considered to be the value at which the frame enters the inelastic range. A drift ratio of 1.5% was determined from the results of a pushover analysis, conducted using the NLFB analysis, for the IO performance level. The LS drift ratio was established as 2% as per FEMA 356 [38] and ASCE 41 [32]. The CP drift ratio was taken as approx. 3%, which represented 75% of the ultimate drift ratio [39].

The fragility curves were derived using a cumulative probability distribution as per Eq. (1).

$$P[d \geq D] = 1 - 1/2\{1 + erf[\ln(D/\mu)/(\beta\sqrt{2})]\} \quad (1)$$

where $P[d \geq D]$ indicates the probability of the defined engineering demand parameters (EDP) (i.e., drift ratio in this study) to exceed the allowable threshold D (i.e., IO, LS, or CP θ_{max}); *erf* is the Gauss error function; μ is the median value of the EDP at a given ground motion intensity; and β is the standard deviation of the natural logarithm of the ground motion index of the damage state. The median value of the EDP is calculated by exponential regression of the θ_{max} - S_a plot (see Fig. 12).

A parametric study using the seven previously selected ground motions was performed. Each ground motion was scaled several times to produce a range of spectral accelerations at the first natural period of the structure. The imposed spectral accelerations were: 0.3 g, 0.6 g, 0.8 g, 1 g, 1.25 g, and 1.5 g. A total of 126 NLDAs were performed (i.e., 42 for each numerical model). Approx. 260 h of analysis time were required to perform all the NLDAs, excluding the model development and result acquisition time.

In Fig. 12a–c, the black diamond-shape points are the recorded maximum first-story drifts calculated by the numerical models on each nonlinear dynamic analysis. The red lines show the standard deviation from the mean, expressed by the red 'x' point. Calculated drifts within the standard deviation lines are considered 'normal', whereas the drifts

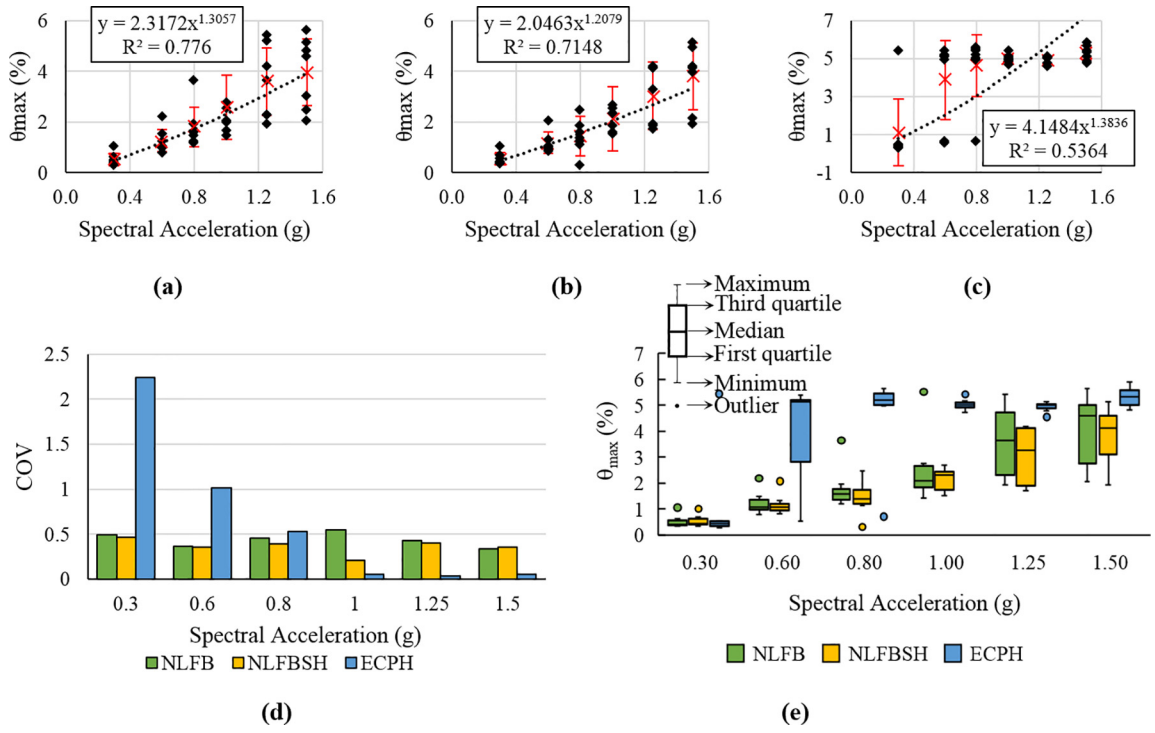

Fig. 12. Calculated structural response for models (a) NLFB, (b) NLFBSH, (c) ECPH, (d) coefficient of variation comparison, and (e) response distribution.

that fall above or below the standard deviation are considered 'abnormally' high or low, respectively, for the collected dataset. The dotted black lines show the exponentially fitted curve from all the first story-drift points, which was used in Eq. (1) to calculate the fragility curves. In Fig. 12c, the variability of the calculated maximum first-story drifts is presented by the means of the coefficient of variation. In Fig. 12d, the statistical box and whiskers plot is presented, where the calculated maximum first-story drift are clustered in their respective quartiles. The outlier data points represent 'abnormal' values, calculated as the drifts that exceeded 1.5 times the interquartile range from the first (if below) or third quartile (if above).

When compared to the NLFB model, the structural response calculated by the NLFBSH model provided a slightly better statistical fit in this study. In Fig. 12a–c, the NLFBSH model had the lowest number of calculated drifts outside the plus or minus standard deviation range (i.e., 6 points compared to 10 from the NLFB model). In Fig. 12d, the NLFBSH model is shown to have a slightly lower coefficient of variation, when compared to the NLFB model. In Fig. 12e, the NLFBSH model calculated three outlier points, while the NLFB model calculated four. The ECPH model provided the poorest data dispersion and curve fitting characteristics of all three models (see Fig. 12c and d). Structural collapses were calculated even at low spectral ground motion acceleration levels: for the spectral acceleration above 1 g, all the ground motions calculated a structural failure. This response of the ECPH model resulted in considerably high drift values. Consequently, the coefficient of variation of the ECPH model up to the 0.8 g spectral acceleration was the highest of all three models while for spectral accelerations above 1 g, the coefficient of variation of the ECPH model was the lowest of all three models. The low calculated coefficient of variations does not mean that the ECPH model was the most precise, but rather that all the calculated drifts were uniformly high (i.e., due to failure), resulting in a low variation.

The developed fragility curves for the three performance levels considered are shown in Fig. 13. When the NLFB and NLFBSH models were considered, the calculated probability of exceedance was similar for all the performance levels, with the highest calculated difference between the models occurring at the CP level. The NLFB model calculated a higher, more conservative probability in all performance levels for lower-to-medium spectral acceleration ground motions whereas, in the high spectral acceleration ranges, the NLFBSH model calculated the highest probability. Fig. 14a shows that the maximum difference in the probability calculated by both models was approx. 20% in all the performance levels. The ECPH model calculated the most conservative results due to the higher overestimation of the drift response of the structure caused by the inability of the ECPH model to redistribute forces once the first hinge fails. It presented a significant deviation from the other two models; the maximum difference in calculated probability of the ECPH and the other two models (see Fig. 14b and c) was approx. 40% and 55% in all performance limits for the NLFB and NLFBSH models, respectively.

The accuracy of the response calculated by the NLFBSH model was similar to that of the NLFB model despite its simplified material model formulation (i.e., no coupled shear effects, no second-order behaviors) and element layout. It should be noted, however, that the frame examined primarily exhibited a column shear failure, which was accounted for the by the NLFBSH model. If other failure mechanisms had played a more significant role, the prediction accuracy of the NLFBSH model would have deteriorated significantly.

8. Summary and conclusions

Three numerical models with different computational demand characteristics were created to evaluate their effectiveness in a performance-based earthquake engineering analysis. A nonlinear fiber-based numerical model (called NLFB), a simplified nonlinear model with coupled axial-flexure and uncoupled shear-hinges (called NLFBSH), and a fully-elastic numerical model with simplified nonlinear plastic hinges (called ECPH) were studied. The performance assessment of a planar reinforced concrete frame was performed employing each numerical model developed. The nonlinear dynamic analysis was performed to verify the accuracy in capturing the experimentally observed behavior and obtain the required computational time demand of each model. A set of seven ground motion acceleration histories were used to determine the calculated performance level, statistical parameters, and

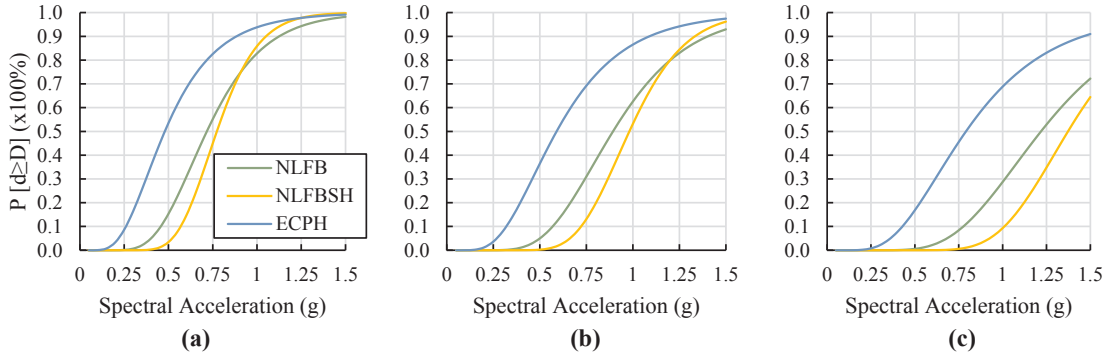

Fig. 13. Fragility functions for the (a) immediate occupancy (IO), (b) life safety (LS), and (c) collapse prevention (CP) performance levels.

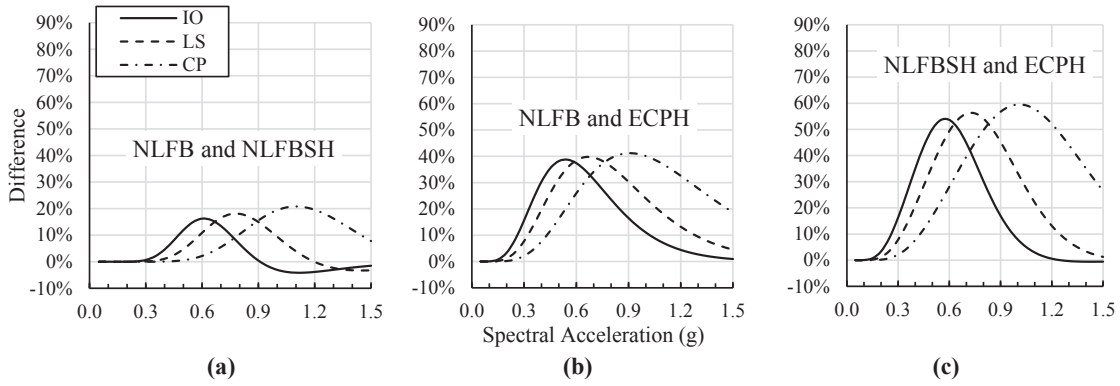

Fig. 14. Calculated probability difference between (a) NLFB and NLFBSH, (b) NLFB and ECPH, and (c) NLFBSH and ECPH numerical models.

derive fragility curves for each of the studied models.

The findings of this study support the following conclusions:

- The developed nonlinear models satisfactorily predicted the drift and base shear responses of the studied structure within 15% deviation from the experimentally observed behavior. The ECPH model significantly underestimated the structural capacity by 40% and the drift response by a factor of four. The inability of the ECPH model to redistribute forces once a plastic hinge fails resulted in the premature termination of the analysis and, thereby, provided an unrealistically high underestimation of the structural capacity.
- The plastic hinges used in the ECPH model could not predict shear failure observed in the experimentally tested specimen. The ECPH model calculated an axial-flexural failure mode, without triggering the shear plastic hinges. Thus, the use of the axial-flexural and shear capacities provided by the ACI building code in the plastic hinges of the ECPH model did not result in an accurate structural response in the dynamic analyses performed.
- The structural response calculated by the NLFB and the NLFBSH model presented a similar overall fit to the four studied statistical parameters, i.e., curve-fitting, number of calculated drifts outside the plus or minus standard deviation range, coefficient of variation, and outlier points. The NLFBSH model however, presented the best statistical fit and, in this study, it was the most suitable model to provide a statistically meaningful performance-based assessment of the studied structure.
- Despite the use of a simplified modeling approach in the NLFBSH model, the fragility curves derived in this study calculated a 20% maximum difference probability between the NLFB and NLFBSH models for all the studied performance limits. Thus, simplified nonlinear models can be used for performance-based analysis to maintain a reasonable level of accuracy while significantly reducing the analysis time demand. Caution should be exercised for cases in which the simplified model may lead to inaccurate results due to the high reliance on the prior knowledge of the governing material behaviors and failure modes, which are not typically known for real structures.
- The fragility curves derived with the ECPH model calculated an unrealistically high probability of structural exceedance of all the three performance limits studied (i.e., immediate occupancy, life safety, and collapse prevention). The reason for this was the combination of the inability of the ECPH model to perform force redistribution once the first plastic hinge failed and the conservative hinge capacity provided by ACI building code.
- When evaluating the required time demand of a numerical model, little or no attention is given to the model development and result acquisition phases. In this study, the model development and result acquisition times represented a significant part of the numerical modeling process, when considered from start to finish. The availability of graphical pre- and post-processor programs and a well-organized user documentation were essential in reducing the model development and result acquisition times. The NLFBSH model, which lacked pre- and post-processors and a well-organized user documentation, required a much longer total time – more than twice that of the NLFB and ECPH models combined – despite having a shorter analysis time.
- The analysis time of each model increased exponentially with the number of material behavior models and elements used. Thus, there is a need for simple but accurate nonlinear dynamic analysis methods due to the large number of analyses required by the performance-based earthquake engineering methodology.

Acknowledgements

The authors would like to thank Wassim M. Ghannoum for providing the experimental shake-table ground motion data for the frame examined in this study.

References

[1] Chen XM, Duan J, Qi H, Li YG. Controls on Material and Mesh for Structural Nonlinear Time-History Analysis. In: Applied Mechanics and Materials, vol. 580, p. 1564–9. Trans Tech Publications 2014.

[2] Möller O, Foschi RO, Quiroz LM, Rubinstein M. Structural optimization for performance-based design in earthquake engineering: Applications of neural networks. Struct Saf 2009;31(6):490–9.

[3] Spacone E, Camata G, Faggella M. Nonlinear models and nonlinear procedures for seismic analysis of reinforced concrete frame structures. Comput Struct Dynam Earthquake Eng: Struct Infrastruct Book Ser 2008;2:323.

[4] Kalkan E, Kunnath SK. Assessment of current nonlinear static procedures for seismic evaluation of buildings. Eng Struct 2007;29(3):305–16.

[5] Ghaffarzadeh H, Talebian N, Kohandel R. Seismic demand evaluation of medium ductility RC moment frames using nonlinear procedures. Earthquake Eng Eng Vibr 2013;12(3):399–409.

[6] Domingues Costa JL, Bento R, Levtchitch V, Nielsen MP. Rigid-plastic seismic design of reinforced concrete structures. Earthquake Eng Struct Dynam 2007;36(1):55–76.

[7] Goel SC, Liao WC, Reza Bayat M, Chao SH. Performance-based plastic design (PBPD) method for earthquake-resistant structures: an overview. Struct Des Tall Special Build 2010;19(1–2):115–37.

[8] Liao WC, Goel SC. Performance-based seismic design of RC SMF using target drift and yield mechanism as performance criteria. Adv Struct Eng 2014;17(4):529–42.

[9] Amouzegar H, Riahi HT. Seismic assessment of concrete frames by endurance time method. Proc Inst Civil Eng-Struct Build 2015;168(8):578–92.

[10] Celik OC, Ellingwood BR. Seismic risk assessment of gravity load designed reinforced concrete frames subjected to Mid-America ground motions. J Struct Eng 2009;135(4):414–24.

[11] Elwood KJ, Moehle JP. Dynamic collapse analysis for a reinforced concrete frame sustaining shear and axial failures. Earthquake Eng Struct Dyn 2008;37(7):991–1012.

[12] Huang X, Kwon OS. Numerical models of RC elements and their impacts on seismic performance assessment. Earthquake Eng Struct Dyn 2015;44(2):283–98.

[13] Zareian F, Krawinkler H. Simplified performance-based earthquake engineering (Doctoral dissertation, Stanford University) 2006.

[14] FEMA. FEMA P-58-1: Seismic Performance Assessment of Buildings. Volume 1–Methodology 2012.

[15] American Society of Civil Engineers. Minimum design loads for buildings and other structures (vol. 7). ASCE Publications 2013.

[16] Council BSS. 2015. NEHRP Recommended Seismic Provisions for New Buildings and Other Structures, Part 1 Provisions, Part 2 Commentary, FEMA Report No. P-1050-1.

[17] PEER. 2017. PEER Ground Motion Database [online]. Available from http://ngawest2.berkeley.edu/ [accessed 16 November 2016].

[18] Ghannoum WM, Moehle JP. Shake-table tests of a concrete frame sustaining column axial failures. ACI Struct J 2012;109(3):393.

[19] Guner S, Vecchio FJ. Pushover analysis of shear-critical frames: formulation. ACI Struct J 2010;107(1):63.

[20] Vecchio FJ, Collins MP. The modified compression-field theory for reinforced concrete elements subjected to shear. ACI J. 1986;83(2):219–31.

[21] Wong PS, Vecchio FJ, Trommels H. VecTor2 and Formworks user's manual, 2013; Rep. Civil Engineering, Univ. of Toronto, Toronto.

[22] Guner S, Vecchio FJ. User's Manual of VecTor5 [online]. The University of Toledo 2008. Available from http://www.utoledo.edu/engineering/faculty/serhan-guner/Publications.html [accessed 23 November 2016].

[23] Guner S. Software [online]. The University of Toledo. 2017. Available from http://www.utoledo.edu/engineering/faculty/serhan-guner/Software.html [accessed 20 November 16].

[24] Sadeghian V. Formworks-Plus: Improved Pre-Processor for Vector Analysis Software. MASc Thesis, Department of Civil Engineering, University of Toronto, Canada, 2012. 147 pp.

[25] Blosser K, Guner S, Vecchio FJ. User's Manual of FormWorks Plus for VecTor5. Online Publication, 2016. 29 pp., http://www.utoledo.edu/engineering/faculty/serhan-guner/Publications.html.

[26] Chak IN. Janus: A Post-Processor for VecTor Analysis Software. MASc Thesis, Department of Civil Engineering, University of Toronto, Canada, 2013. 193 pp.

[27] Loya AS, Lourenço DDS, Guner S, Vecchio FJ. User's Manual of Janus for VecTor5. Online Publication, 2017. 28 pp. http://www.utoledo.edu/engineering/faculty/serhan-guner/Publications.html.

[28] Vecchio FJ. Towards cyclic load modeling of reinforced concrete. ACI Struct J 1999;96:193–202.

[29] Seckin M. Hysteretic Behaviour of Cast-in-Place Exterior Beam-Column-Slab Subassemblies. PhD thesis, Department of Civil Engineering, University of Toronto, Toronto, Ontario, Canada, 1981, 266 pp.

[30] LeBorgne MR, Ghannoum WM. Analytical element for simulating lateral-strength degradation in reinforced concrete columns and other frame members. J Struct Eng 2013;140(7):04014038.

[31] Mazzoni S, McKenna F, Scott MH, Fenves GL. OpenSees command language manual. Pacific Earthquake Engineering Research (PEER) Center; 2006.

[32] American Society of Civil Engineers. Seismic rehabilitation of existing buildings (vol. 41, No. 13). ASCE Publications; 2014.

[33] Filippou F. Concrete02 Material – Linear Tension Softening. OpenSeesWiki; 2010. Available from http://opensees.berkeley.edu/wiki/index.php/Concrete02_Material_-_Linear_Tension_Softening [accessed 20 November 2016].

[34] Mander JB, Priestley MJ, Park R. Theoretical stress-strain model for confined concrete. J Struct Eng 1988;114(8):1804–26.

[35] Csi C. Analysis reference manual for SAP2000, ETABS, and SAFE. California, USA: Computers and Structures Inc; 2015.

[36] ACI Committee, American Concrete Institute, & International Organization for Standardization. Building code requirements for structural concrete (ACI 318-14) and commentary. American Concrete Institute; 2014.

[37] Guner S, Vecchio FJ. Simplified method for nonlinear dynamic analysis of shear-critical frames. ACI Struct J-Am Concr Inst 2012;109(5):727.

[38] FEMA. Pre-standard and Commentary for the Seismic Rehabilitation of Buildings (FEMA-356); 2000.

[39] Erberik MA. Fragility-based assessment of typical mid-rise and low-rise RC buildings in Turkey. Eng Struct 2008;30(5):1360–74.